The Plant Cell, Vol. 28: 1297–1309, June 2016, www.plantcell.org

Identification and Characterization of Maize *salmon silks* Genes Involved in Insecticidal Maysin Biosynthesis[OPEN]

María Isabel Casas,[a,b] María Lorena Falcone-Ferreyra,[c] Nan Jiang,[b] María Katherine Mejía-Guerra,[a,b] Eduardo Rodríguez,[d] Tyler Wilson,[b] Jacob Engelmeier,[b] Paula Casati,[c] and Erich Grotewold[b,e,1]

[a] Molecular, Cellular, and Developmental Biology Program, The Ohio State University, Columbus, Ohio 43210
[b] Center for Applied Plant Sciences, The Ohio State University, Columbus, Ohio 43210
[c] Centro de Estudios Fotosintéticos y Bioquímicos, Universidad Nacional de Rosario, Santa Fe S2002LRK, Argentina
[d] Instituto de Biología Molecular y Celular de Rosario, Rosario, Santa Fe S2002LRK, Argentina
[e] Department of Molecular Genetics, The Ohio State University, Columbus, Ohio 43210

ORCID IDs: 0000-0002-1395-9646 (M.I.C.); 0000-0002-7283-6347 (N.J.); 0000-0002-2791-182X (M.K.M.-G.); 0000-0002-9467-8909 (T.W.); 0000-0002-3194-4683 (P.C.)

The century-old maize (*Zea mays*) *salmon silks* mutation has been linked to the absence of maysin. Maysin is a *C*-glycosyl flavone that, when present in silks, confers natural resistance to the maize earworm (*Helicoverpa zea*), which is one of the most damaging pests of maize in America. Previous genetic analyses predicted *Pericarp Color1* (*P1*; R2R3-MYB transcription factor) to be epistatic to the *sm* mutation. Subsequent studies identified two loci as being capable of conferring *salmon silks* phenotypes, *salmon silks1* (*sm1*) and *sm2*. Benefitting from available *sm1* and *sm2* mapping information and from knowledge of the genes regulated by *P1*, we describe here the molecular identification of the *Sm1* and *Sm2* gene products. *Sm2* encodes a rhamnosyl transferase (UGT91L1) that uses isoorientin and UDP-rhamnose as substrates and converts them to rhamnosylisoorientin. *Sm1* encodes a multidomain UDP-rhamnose synthase (RHS1) that converts UDP-glucose into UDP-L-rhamnose. Here, we demonstrate that RHS1 shows unexpected substrate plasticity in converting the glucose moiety in rhamnosylisoorientin to 4-keto-6-deoxy glucose, resulting in maysin. Both *Sm1* and *Sm2* are direct targets of P1, as demonstrated by chromatin immunoprecipitation experiments. The molecular characterization of *Sm1* and *Sm2* described here completes the maysin biosynthetic pathway, providing powerful tools for engineering tolerance to maize earworm in maize and other plants.

INTRODUCTION

Maize (*Zea mays*) is one of the most cultivated cereals worldwide, covering ~40% of the global arable land, a consequence of its nutritional value as a feeding crop and feedstock. In addition, it is utilized for biofuels, plastic, fabric production, and by the food industry (Morris and Sands, 2006). The process of selective breeding applied to increased productivity, high kernel quality for better edibility, increased starch content, thin pericarps surrounding kernels, and loose husks to allow easier drying of the cob has resulted in the increased susceptibility of maize to several pests (Bailey and Bailey, 1938). Chief among them is damage by the lepidopteran maize earworm (CEW, *Helicoverpa zea* Boddie), responsible for significant grain losses in the US. CEW destruction starts when the newly hatched larvae start feeding on silks, the elongated stigmas on the female flower, until they reach the ear and continue to feed on kernels (Waiss et al., 1979). Antibiosis to CEW is primarily provided by maysin [2′′-*O*-α-rhamnosyl-6-*C*-(6-deoxy-xylo-hexos-4-ulosyl)luteolin] (Waiss et al., 1979), a *C*-glycosyl flavone with strong feeding deterrent effects, first characterized from the Mexican maize landrace Zapalote Chico (Elliger, 1980; Wiseman et al., 1992; Widstrom and Snook, 1998a, 1998b).

Given the devastating effects of CEW, efforts involving quantitative trait locus mapping were performed to identify specific genomic regions responsible for regulating the accumulation of maysin and therefore increasing natural resistance to CEW. A region in the short arm of chromosome 1 accounted for more than half of the phenotypic variance (Byrne et al., 1996). This genomic region harbors the *pericarp color1* (*P1*) locus, encoding an R2R3-MYB transcription factor (Grotewold et al., 1991) that, when expressed in maize Black Mexican Sweet cells, was sufficient to induce the formation of *C*-glycosyl flavones (Grotewold et al., 1998). *P1* had been known for over a century for its ability to control the accumulation of the brick-red phlobaphene pigments in pericarp and cob glume tissues (Emerson, 1917; Anderson and Emerson, 1923), which are a landmark of 'Indian Maize'. Phlobaphenes result from the polymerization of luteoforol (or apiforol), a flavan-4-ol derived from eriodictyol (or naringenin) by the action of dihydroflavonol-4-reductase, encoded by the *A1* gene (Figure 1). Alternatively, luteoforol can be converted to the 3-deoxy anthocyanidin luteolinidn by an unknown enzyme, probably with anthocyanidin synthase-like activity (Figure 1). *P1* alleles can cause red pigment to accumulate in the pericarp and the cob glumes (*P1-rr*, for red pericarp and red cob), only the cob glumes (*P1-wr*, for white pericarp and red cob), only the pericarp (*P1-rw*, for red pericarp and white cob), or

[1] Address correspondence to grotewold.1@osu.edu.
The author responsible for distribution of materials integral to the findings presented in this article in accordance with the policy described in the Instructions for Authors (www.plantcell.org) is: Erich Grotewold (grotewold.1@osu.edu).
[OPEN]Articles can be viewed without a subscription.
www.plantcell.org/cgi/doi/10.1105/tpc.16.00003

neither the cob glumes nor the pericarp (*P1-ww*, for white pericarp and white cob).

Maysin biosynthesis involves the conversion of eriodictyol to 2-hydroxyeriodictyol by the *P1*-regulated flavanone 2-hydroxylase (F2H1, CYP93G5; Morohashi et al., 2012). Subsequently, 2-hydroxyeriodictyol is *C*-glycosylated by the *C*-glucosyl transferase UGT708A6 (Falcone Ferreyra et al., 2013), and following a likely spontaneous dehydration reaction (Brazier-Hicks et al., 2009), isoorientin (luteolin 6-*C*-glucoside) is formed (Figure 1). From the structures determined by McMullen et al. (2004) using NMR, the conversion of isoorientin to maysin requires at least two additional enzymatic steps: the first one involving the incorporation of a rhamnose to the glucose moiety of isoorientin to form rhamnosylisoorientin (isoorientin 2′′-*O*-rhamnoside) and the second involving the dehydration of glucose to 4-keto-6-deoxy glucose to convert rhamnosylisoorientin into maysin (Figure 1). The enzymes responsible for these last steps in the maysin biosynthetic pathway remain unknown, but they were proposed to correspond to the *salmon silks* loci (McMullen et al., 2004). The original *salmon silks* mutant (currently known as *sm1*) was originally identified at a Nebraska fair in 1909 (Anderson, 1921); their name describes the characteristically strong salmon-colored silks of these lines, compared with the usual green or purple color of silks. So far, two *salmon silks* loci have been identified, *sm1* (on the long arm of chromosome 6) and *sm2*, on the long arm of chromosome 2 (Anderson, 1921; McMullen et al., 2004).

Here, we describe the cloning and biochemical characterization of *Sm1* and *Sm2*, resulting in the completion of the maysin biosynthetic pathway. Selecting *P1*-regulated genes in the *sm1* and *sm2* respective mapping intervals identified candidate genes, which were further tapered by testing whether mRNA accumulation was affected in the respective mutants. To unequivocally demonstrate the identity of the identified genes as *Sm1* and *Sm2*, we developed a maize biochemical complementation system consisting of *sm1* or *sm2* protoplasts, which upon transformation with P1, accumulate metabolic intermediates corresponding to where the pathway is blocked in each mutant. Complementation by transformation with the candidate genes hence results in flux through the pathway being restored and maysin accumulation. Using this approach, we show here that *Sm2* encodes a rhamnosyl transferase (UGT91L1) that uses UDP-rhamnose (UDP-Rha) and isoorientin as substrates, producing rhamnosylisoorientin. In turn, *Sm1* encodes an UDP-rhamnose synthase (RHS1), which in a very unusual reaction converts the glucose moiety in rhamnosylisoorientin to 4-keto-6-deoxy glucose, resulting in maysin formation. Thus, an elegant combination of genetics, high-throughput sequencing, and biochemistry permitted us to identify elusive genes responsible for the last biosynthetic steps of an agronomically important antibiosis compound.

RESULTS

Biochemical Validation of Flavonoids Accumulating in *sm* Silks

Previous studies had identified the main flavones accumulating in *sm1* and *sm2* mutants (McMullen et al., 2004). To obtain a baseline flavone profile for the other experiments described in this study, we obtained seeds for different *sm* alleles from the Maize Genetics Cooperation Stock Center. For simplicity, we named those alleles *sm1-1* through *sm1-8*, and *sm2-1* through *sm2-5* (Supplemental Table 1). Visual kernel and cob inspection of each mutant line permitted us to establish the most likely *P1* allele present in each one (Supplemental Table 1). To determine whether the various *sm2* and *sm1* lines accumulated the expected pathway intermediates, isoorientin (IO) for *sm2* and rhamnosylisoorientin (RIO) for *sm1* (McMullen et al., 2004; Figure 2A), we performed HPLC analysis following absorbance at 350 nm on silk methanolic extracts and compared the retention times on each chromatographic profile with those of available authentic standards. Silk extracts from the *sm2-1* mutant (Figure 2B) and other *sm2* alleles (Supplemental Figure 1) show a peak at 5.2 min, corresponding to IO, and little to no accumulation of RIO or maysin, which are highly accumulated in *P1-rr* (expressing *Sm1* and *Sm2*) silks (Figure 2B). The peak at ~7 min may correspond to derhamnosylmaysin (Figure 2B), which was previously identified in *sm2* silks and proposed to be a product of *sm1* acting on IO instead of RIO (McMullen et al., 2004).

Silk extracts from the *sm1-3* mutant (Figure 2B) and other *sm1* alleles (Supplemental Figure 2) show a peak at 4.5 min, corresponding to RIO, which is absent in *P1-rr Sm1* silks (Figure 2B, third panel). In addition, silks from *sm1-1* mutants show the presence of variable amounts of maysin (Supplemental Figure 2), suggesting that the respective *sm1* alleles are not complete loss of function.

To determine whether the ectopic expression of *P1* in the respective mutants recapitulates the accumulation of pathway intermediates present in *sm1* and *sm2* silks, we developed a transformation system using maize protoplasts obtained from *sm* mutant seedlings. Extracted flavonoids from protoplasts isolated from *sm2-1* or *sm1-3* seedlings transformed with a negative control were analyzed by liquid chromatography followed by tandem mass spectrometry (LC-MS/MS) and showed trace levels of IO and RIO, respectively (Figure 2C, second and fourth panels). This is consistent with *P1* not normally being expressed in maize vegetative tissues (Sidorenko et al., 2000; Cocciolone et al., 2001). Transformation with P1 expressed from the constitutive *CaMV 35S* promoter ($35S_{pro}$:P1) resulted in a significant accumulation of IO in *sm2-1* and of both IO and RIO in *sm1-3* (Figure 2C), indicating that the presence of P1 in seedling protoplasts is sufficient to recapitulate precursor accumulation similarly to what happens in silks. Taken together, these results confirm that *sm2* is blocked in the conversion of IO to RIO and *sm1* in the conversion of RIO to maysin and that *P1* is epistatic to both *sm1* and *sm2*.

Identification and Characterization of *sm2* Candidate Genes

The *sm2* locus maps between the *phi127* and *bnlg1721* markers on the long arm of chromosome 2 (T218 × GT119 F2, 1997 map; McMullen et al., 2004). This region corresponds to ~11 Mb, and the available draft maize genome sequence (Maize B73 RefGen v2) shows 336 putative genes from the working gene set in this interval (Figure 3A). Taking advantage of previous mRNA-sequencing (RNA-seq) information from contrasting *P1-rr* and *P1-ww* silks and pericarps at different developmental stages (Morohashi et al., 2012), we investigated which of these 336 genes

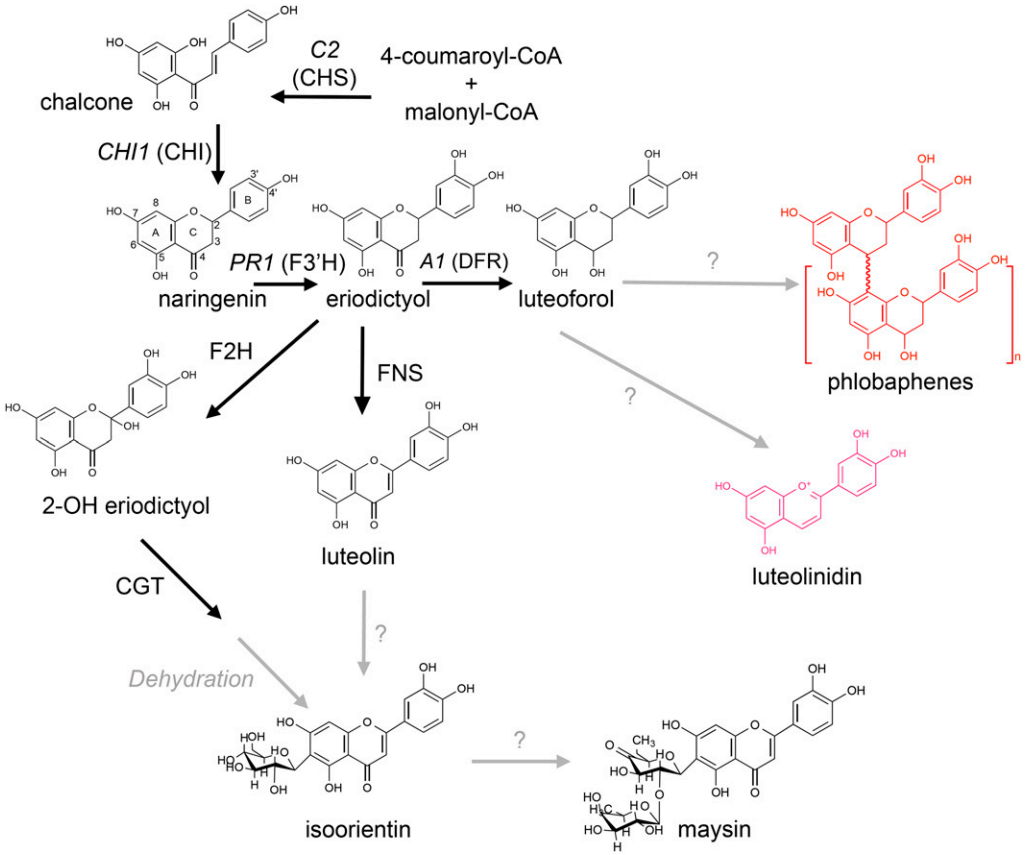

Figure 1. Proposed 3-Deoxyflavonoid Biosynthetic Pathway.

Condensation of *p*-coumaroyl-CoA and malonyl-CoA by chalcone synthase (CHS; *C2*) results in naringenin chalcone, which is then converted to naringenin by chalcone isomerase (CHI; encoded by *CHI1*). Naringenin is converted to eriodictyol by a flavanone-3′-hydroxylase (F3′H1; encoded by *PR1*), which could then be converted to the flavone luteolin by a flavone synthase (FNS; *FNSI-1*) (Falcone Ferreyra et al., 2015). Eriodictyol is converted to isoorientin (*C*-glycosyl flavone) by a flavanone-2-hydroxylase (F2H; *CYP93G5*) (Morohashi et al., 2012) and a *C*-glucosyl transferase (CGT; *UGT708A6*) (Falcone Ferreyra et al., 2013). The proposed steps for conversion of isoorientin to maysin involve at least two enzymatic conversions by as yet uncharacterized enzymes. Eriodictyol is also converted to luteoforol (flavan-4-ol) by a dihydroflavonol reductase (DFR; *A1*) and subsequently to luteolinidin (3-deoxy anthocyanidin) by what is thought to be an ANS-like enzyme (Liu et al., 2010) or is polymerized into phlobaphenes. Enzymes identified are shown in black, and proposed steps are in gray. Phlobaphenes are shown in red, and 3-deoxyanthocyanidins are shown in pink.

showed an increase in mRNA accumulation in *P1-rr* compared with *P1-ww*, comparable to other flavonoid pathway genes (e.g., *C2*, encoding chalcone synthase, and *A1*; Figure 3A). Of the 336 gene models contained in the *sm2* mapping interval (Figure 3A; Supplemental Table 2), mRNA levels for nine genes were significantly higher in *P1-rr* compared with *P1-ww* silks (Supplemental Table 2). Sequence analyses from proteins encoded by these genes yielded UGT91L1 (GRMZM2G180283) as a putative UDP-glycosyltransferase (UGT) that clustered together with previously characterized UGTs that use flavonoid glycosides as substrate acceptors and catalyze the formation of sugar-*O*-sugar links, including the rhamnosyl transferases from *Petunia hybrida* and *Citrus maxima* (Falcone Ferreyra et al., 2013). Moreover, in phylogenetic analyses of all putative maize UGTs, five additional UGTs clustered together with UGT91L1, but none of the genes encoding these UGTs are upregulated by *P1* in silks, further supporting UGT91L1 as an *Sm2* candidate (Supplemental Figure 3 and Supplemental Data Set 1).

We rationalized that if *UGT91L1* corresponds to *Sm2*, then the *UGT91L1* gene could be mutated, and/or *UGT91L1* mRNA levels could be reduced in the *sm2* mutant alleles. To test this, we sequenced the genomic region corresponding to *UGT91L1* to ~1.5 kb upstream of the predicted transcription start site and identified several nucleotide differences with the B73 reference allele primarily located in the upstream regulatory region, but none resulting in an amino acid change (Supplemental Figure 4A and Supplemental Table 7). Since the genetic background of the *sm* mutants is not known, these DNA sequence differences with B73 (shared between all sequenced *sm2* alleles) could correspond to genetic background differences and not necessarily be responsible for the *sm2* phenotypes. To evaluate whether *UGT91L1* mRNA levels are reduced, we performed RT-qPCR on cDNA obtained from silk tissues from the various *sm2* alleles using three different primers sets and compared mRNA levels to those in *P1-rr* and *P1-ww* silks, in which a wild-type *Sm2* allele is present (as positive and negative controls, respectively; Supplemental Figure 4 and

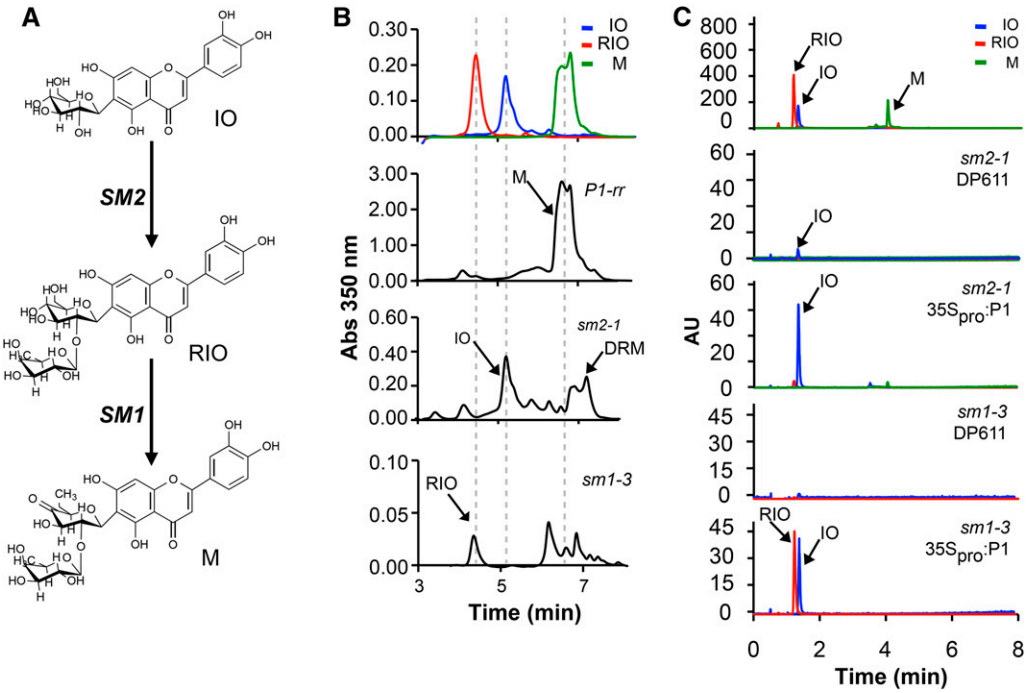

Figure 2. Biochemical Analysis of *sm* Lines.

(A) Proposed pathway for maysin formation. The reaction from IO to RIO is proposed to be mediated by *sm2* and the dehydration of RIO to maysin (M) by *sm1*.
(B) HPLC chromatograms of methanolic extracts from *salmon silks* mutant silks following absorbance at 350 nm. Upper panel: IO (blue), RIO (red), and maysin (green) standards. Second panel: extracts from *P1-rr* silks, in which *sm2* and *sm1* are active, accumulate maysin. Third panel: *sm2* mutant extracts from *sm2-1* silks accumulate IO. Lower panel: *sm1* mutant extracts from *sm1-3* silks accumulate RIO.
(C) Upper panel: LC-MS/MS profiles following m/z^- ratios of 447 for IO, 593 for RIO, and 574 for maysin standards. Second and third panels depict representative LC-MS/MS profiles of *sm2* protoplast extracts transformed with the negative control (DP611) and with $35S_{pro}$:P1 showing the m/z^- 447 molecular ion corresponding to IO. Fourth and fifths panels depict representative LC-MS/MS profiles of *sm1* protoplast extracts transformed with the negative control (DP611) or with $35S_{pro}$:P1 showing the m/z^- 447 and 593 molecular ions corresponding to IO and RIO, respectively.

Supplemental Table 6). Consistent with the flavone profile analyses indicating the absence of maysin in silks from *sm2-1*, *sm2-2*, and *sm2-5* and a significant reduction in *sm2-3* (Figure 2; Supplemental Figure 1), RT-qPCR experiments showed an almost complete absence of *UGT91L1* transcripts in silks of these mutant lines (Supplemental Figure 4B). Thus, given the high identity with rhamnosyl transferases, the location in the *sm2* interval, the regulation by *P1*, and the reduced expression in several *sm2* mutant alleles, our results strongly suggest that *UGT91L1* is a good candidate for *Sm2*.

UGT91L1 Encodes a Rhamnosyl Transferase That Complements the *sm2* Mutation

To determine whether UGT91L1 is able to carry out the rhamnose addition required for the conversion of IO to RIO (Figure 2A), we cloned the full open reading frame of UGT91L1 in the pET28a vector (Figure 3B) and expressed the encoded protein in *Escherichia coli* as an N-terminal fusion protein with a six-histidine tag (His_6-UGT91L1; see Methods).

We anticipated that, in addition to IO, a reaction involving UGT91L1 would require UDP-Rha as a substrate, which is not commercially available. Thus, to generate UDP-Rha, we cloned a previously characterized rhamnose synthase from *Arabidopsis thaliana* (At-RHM1) into the pGZ25 vector and transformed it into the T334 yeast strain (Watt et al., 2004; Oka et al., 2007). Crude protein extracts from yeast cells transformed with the empty vector (see Methods) were used as negative control. Total protein extracts from yeast cultures expressing At-RHM1 and supplied with UDP-glucose (UDP-Glu), NAD^+, and NADPH (Oka et al., 2007) were used to obtain UDP-Rha. Subsequently, total protein extracts from *E. coli* cultures expressing UGT91L1 were assayed for rhamnosyl transferase activity by incubation with IO and the UDP-Rha previously generated. LC-MS/MS analyses indicated that UGT91L1 produced a compound (with a retention time of ~2.5 min), absent when only the empty plasmid was used (compared with the second and third panels in Figure 3B), with an m/z of 595.2 that was identified as RIO, by comparison with the respective standard.

To unequivocally demonstrate that UGT91L1 corresponds to *Sm2*, we investigated whether UGT91L1 complemented the *sm2* mutation, taking advantage of the maize protoplast transformation system described above. To this end, we cloned the full open reading frame of UGT91L1 as a C-terminal translational fusion to enhanced GFP, expressed under the control of the 35S promoter ($35S_{pro}$:UGT91L1-GFP; Supplemental Figure 5A). We transformed *sm2-1* protoplasts with $35S_{pro}$:P1, with and without $35S_{pro}$:UGT91L1-GFP. After transformation, methanolic extracts were analyzed for RIO accumulation by LC-MS/MS. As shown in Figure

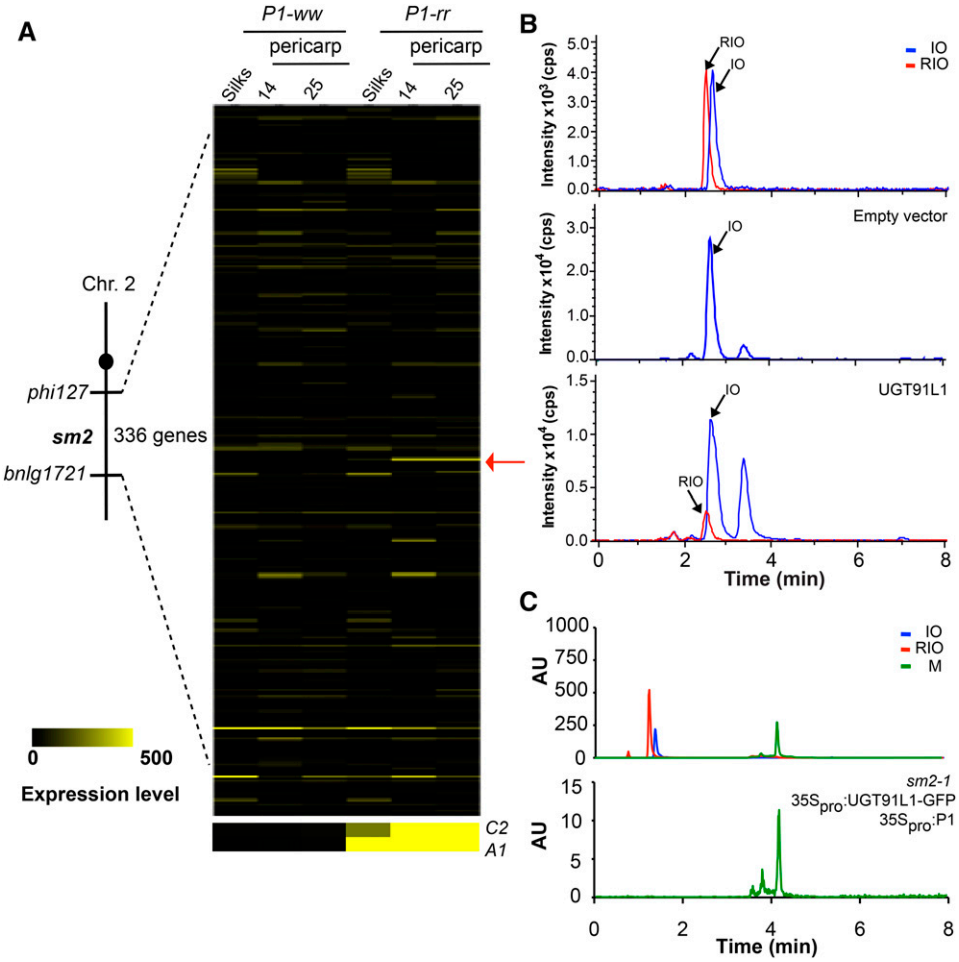

Figure 3. UGT91L1 Corresponds to the *sm2* Locus.

(A) The *sm2* mapping region on chromosome 2 covers an 11-Mb region between markers *phi127* and *bnlg1721* comprising 336 gene models, out of which a putative glycosyl transferase (UGT91L1, GRMZM2G180283; red arrow) was identified as a candidate. *A1* and *C2* levels are shown as reference for the expression of other flavonoid genes upregulated by P1. Expression levels are in FPKM (fragments per kilobase of transcript sequence per million base pairs sequenced).

(B) LC-MS/MS analysis of in vitro UGT91L1 activity assayed using UDP-Rha and IO as substrates showing the production of a molecular ion of m/z^+ 595 (lower panel) that corresponds to RIO compared with the corresponding standard (upper panel), confirming that UGT91L1 functions as Sm2. *E. coli* cells transformed with the empty vector (pET28) did not show the production of this compound (middle panel). Upper panel: representative ion chromatograms of true standards IO (blue, $m/z^+ = 449$) and RIO (red, $m/z^+ = 595$).

(C) LC-MS/MS analysis shows that maysin accumulation following $m/z^- = 574$ is reconstituted in *sm2-1* protoplasts cotransformed with $35S_{pro}$:UGT91L1-GFP and $35S_{pro}$:P1 (lower panel) but not with $35S_{pro}$:P1 alone (Figure 2C). Upper panel: representative ion chromatograms following the *m/z* ratios of true standards IO (blue, $m/z^- = 447$), RIO (red, $m/z^- = 593$), and maysin (green, $m/z^- = 574$).

3C, maysin is present in the $35S_{pro}$:P1 transformed protoplasts only if $35S_{pro}$:UGT91L1-GFP was present as well (Figure 3C, second panel, negative control). Taken together, our results demonstrate that *UGT91L1* encodes a functional rhamnosyl transferase that uses IO as substrate and that it biochemically complements the *sm2* mutation. Thus, UGT91L1 corresponds to Sm2.

Identification and Characterization of *sm1* Candidate Genes

To molecularly characterize *sm1*, we determined that the genetic interval that contains this locus (Anderson, 1921), and which spans the region between *tangled1* (*tan1*) to *purple plant1* (*pl1*) loci on chromosome 6, corresponds to ~35 Mb and contains ~797 gene models (Genetic Map 2008; Wei et al., 2009; Figure 4A).

Similarly as we did for *sm2*, we determined that 27/797 gene models were expressed significantly higher in *P1-rr* compared with *P1-ww* silks (Figure 4A; Supplemental Table 3). Within the genes in the *sm1* interval, GRMZM2G031311 was particularly attractive as an *sm1* candidate because sequence analyses indicated it encoded a putative rhamnose synthase with 79.8% identity and 88.0% similarity at the amino acid level with At-RHM1 (Rice et al., 2000) and which we called RHS1. The conversion of

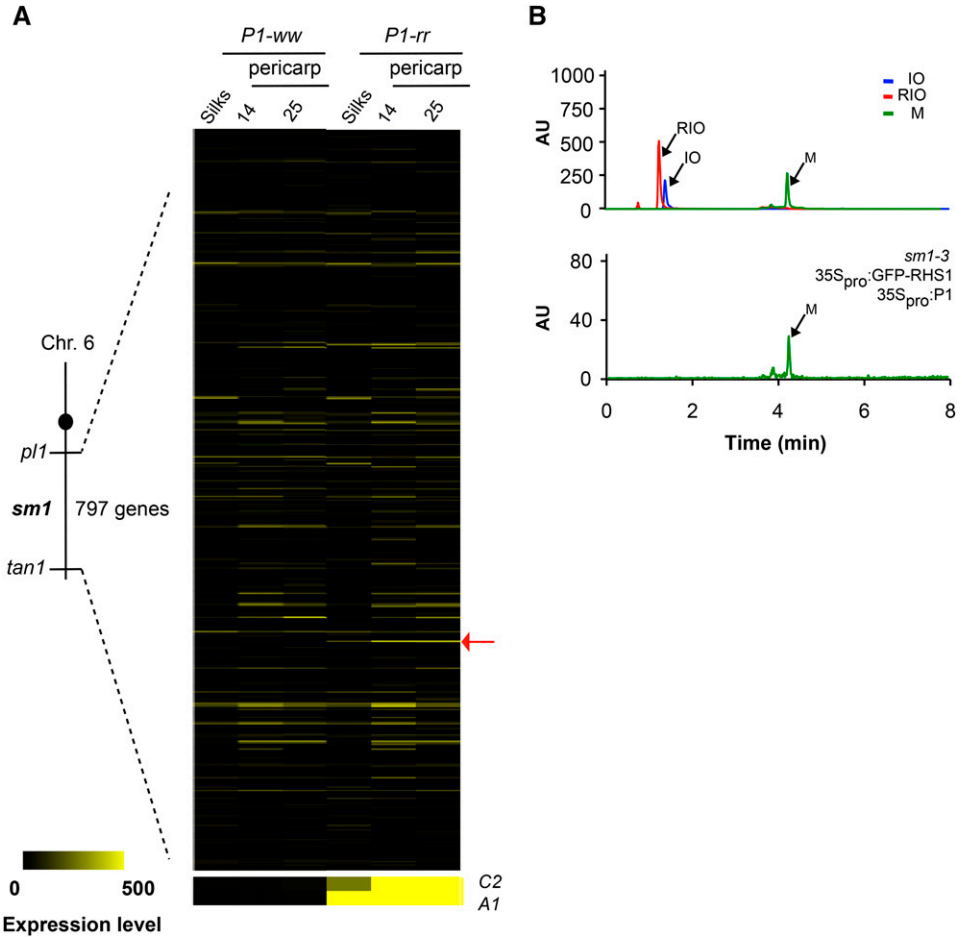

Figure 4. RHS1 Is a Strong *sm1* Candidate.

(A) The *sm1* mapping region on chromosome 6 covers a 35.5-Mb region between *pl1* and *tan1* comprising 797 gene models, from which a putative UDP-rhamnose synthase (RHS1, GRMZM2G031311; red arrow) was identified as a candidate. *A1* and *C2* levels are shown as reference for the expression of other flavonoid genes upregulated by P1. Expression levels are in FPKM (fragments per kilobase of transcript sequence per million base pairs sequenced).
(B) LC-MS/MS analysis following m/z^- of 574 shows that maysin accumulation is reconstituted in *sm1-3* protoplasts cotransformed with $35S_{pro}$:GFP-RHS1 and $35S_{pro}$:P1 but not with $35S_{pro}$:P1 alone (Figure 2C). Upper panel: representative ion chromatograms following the *m/z* ratios of true standards IO (blue, $m/z^- = 447$), RIO (red, $m/z^- = 593$), and maysin (green, $m/z^- = 574$).

UDP-Glu to UDP-Rha by rhamnose synthases involves a first step that results in UDP-4-keto-6-deoxy glucose catalyzed by the N-terminal domain with dehydratase activity, which is then converted into UDP-Rha by the action of the epimerase/reductase activity of the C-terminal domain (Figures 5A and 5B; Giraud and Naismith, 2000). Because the conversion of RIO into maysin involves the dehydration of the glucose group in RIO to 4-keto-6-deoxy glucose, RHS1 provided a good candidate for *sm1* (Figures 2A and 5C). To further support the identity of RHS1 as Sm1, we analyzed all putative rhamnose synthase genes present in the maize genome (Supplemental Table 4). We found three additional genes encoding putative RHMs, but none of them are in the *sm1* interval or are as significantly regulated by P1 as *RHS1*. These results supported RHS1 as a possible Sm1 candidate (Supplemental Table 2). Nevertheless, the remaining genes could potentially provide the UDP-Rha to be used as substrate by UGT91L1, in addition to other metabolic functions.

To investigate the nature of the *sm1* mutations, we sequenced the *RHS1* regions in *sm1-1*, *sm1-2*, *sm1-3*, and *sm1-6*, up to 2 kb upstream of the TSS. While we found no nucleotide differences between *sm1-6* and the B73 reference allele in the 5.6 kb of genomic region sequenced, several nucleotide changes were evident in *sm1-1*, *sm1-2*, and *sm1-3* (Supplemental Figure 6A and Supplemental Table 7). One of those changes in *sm1-3* resulted in the replacement of Met-525 to Leu. Met-525 is conserved in all plant RHMs so far characterized, suggesting an important functional role (Yin et al., 2011; Reiter and Vanzin, 2001). The other changes (shared between both alleles) are in the region upstream of the TSS or result in conservative changes that do not affect the protein sequence (Supplemental Figure 6A).

To determine whether *RHS1* mRNA accumulation is affected in the *sm1* mutants, we performed RT-qPCR experiments using cDNA obtained from silks from *sm1-1*, *sm1-3*, and *sm1-6* and *RHS1*-specific primers, normalized to *actin1*. All experiments

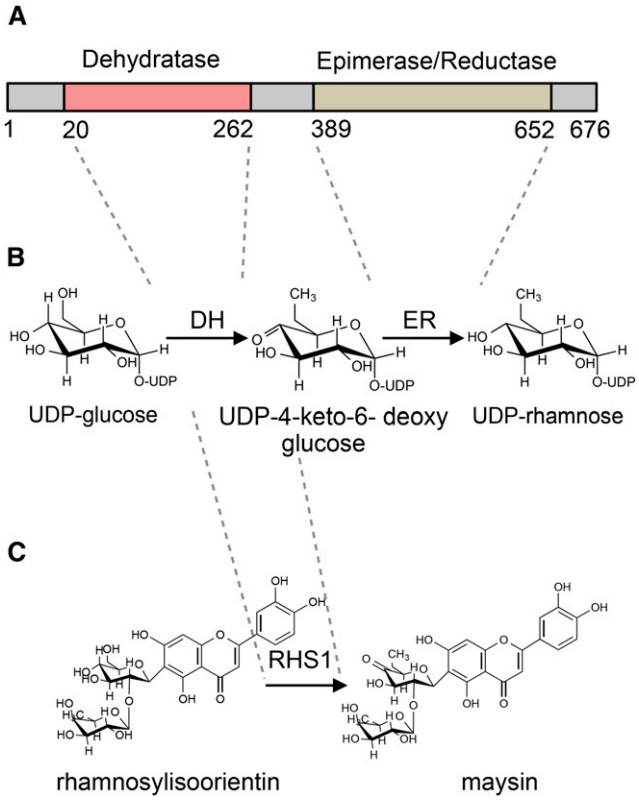

Figure 5. Proposed Mechanism for RHS1 as *sm1* Candidate.

RHS1 contains two domains characteristic of plant rhamnose synthases.
(A) The N-terminal domain between residues 20 and 262 corresponds to a NAD^+-dependent dehydratase and the C-terminal domain corresponds to an epimerase/reductase between residues 389 and 652.
(B) UDP-rhamnose biosynthesis starts with a dehydration step to form the UDP-4-keto-6-deoxy glucose intermediate, which is then converted to UDP-rhamnose by an epimerization reduction step.
(C) Proposed mechanism for RHS1 involvement in maysin biosynthesis by dehydrating the glucose moiety in rhamnosylisoorientin.

were performed in biological triplicate using three sets of primers (Supplemental Figure 6A and Supplemental Table 6). We compared mRNA levels to those in *P1-rr* and *P1-ww*, both lines with a wild-type allele of *Sm1* (as positive and negative controls, respectively; Supplemental Figure 6). Consistent with the HPLC results that showed that these alleles accumulated reduced levels of maysin (Supplemental Figure 2), *sm1-6* accumulated low *RHS1* mRNA levels (Supplemental Figure 6). By contrast, *sm1-1* accumulated higher levels of *RHS1* mRNA than those present in *P1-ww*, but lower than those in *P1-rr* (Supplemental Figure 6). These results suggest that *RHS1* is a candidate gene for the *Sm1* locus.

RHS1 Complements *sm1* Mutants

To unequivocally determine whether *RHS1* corresponds to *Sm1*, we investigated whether RHS1 complements *sm1* using the maize protoplast system described for *sm2*. Cotransformation with $35S_{pro}$:P1 and $35S_{pro}$:RHS1-GFP (Supplemental Figure 5B), but not with $35S_{pro}$:P1 (Figure 2C, third panel) or $35S_{pro}$:RHS1-GFP alone, resulted in *sm1-3* protoplasts that accumulate maysin (Figure 4B), as determined by LC-MS/MS analyses following the *m/z* 577 molecular ion corresponding to the M standard. These results confirm that *RHS1* corresponds to *Sm1*.

Sm2 and *Sm1* Are Direct Targets of P1

UGT91L1 and *RHS1* were selected as *Sm2* and *Sm1* gene candidates, respectively, because RNA-seq experiments showed the respective mRNAs to be significantly higher in *P1-rr* compared with *P1-ww* (Figures 3A and 4A). In addition, the mRNA levels from these genes were reduced in the respective *sm* mutants as confirmed by the RT-qPCR results described above (Supplemental Figures 4 and 6). Finally, complementation experiments further confirmed the identities of these two genes. To investigate whether *UGT91L1* and *RHS1* are P1 direct targets as is the case for other genes involved in 3-deoxyflavonoid and flavone biosynthesis (Morohashi et al., 2012), we conducted chromatin immunoprecipitation (ChIP) experiments using a polyclonal antibody specific for P1 (Falcone Ferreyra et al., 2010; Morohashi et al., 2012), followed by quantitative PCR (ChIP-qPCR) using primers close to or flanking P1 binding sites (Morohashi et al., 2012). Our results show a specific enrichment of the upstream regulatory sequences of *UGT91L1* and *RHS1* (Figure 6) in ChIP experiments conducted on *P1-rr*, but not *P1-ww*, pericarps (Figure 6). Taken together, our results demonstrate that, similarly to other genes involved in flavonoid biosynthesis so far identified, P1 directly regulates the expression of *UGT91L1* (*Sm2*) and *RHS1* (*Sm1*) in pericarps and silks of maize, resulting in the accumulation of maysin.

DISCUSSION

As has been the case for many other maize flavonoid genes (Coe, 2001), the distinctive color of 3-deoxyanthocyanidins provided by the *sm* mutations (Levings, 1972) permitted us to unequivocally characterize the last two enzymatic steps in the maysin biosynthetic pathway, corresponding to Sm2 and Sm1. *Sm2* encodes a rhamnosyl transferase (UGT91L1) that forms rhamnosylisoorientin from UDP-Rha and isoorientin. In turn, rhamnosylisoorientin is the substrate for the rhamnose synthase (RHS1) encoded by *Sm1*, which converts it into maysin. To demonstrate the molecular identity of *UGT91L1* as *Sm2* and *RHS1* as *Sm1*, we developed a maize protoplast complementation system that circumvents the need for transgenic plants. This approach could be easily adapted to probe the activity of other metabolic enzymes. These studies, together with our previous characterization of CYP93G5 that converts flavanones (including naringenin and eriodictyol) to the respective 2-hydroxyflavanones (Morohashi et al., 2012) and UGT708A6 that *C*-glycosylates 2-hydroxyflavanones to the respective flavone-6-*C*-glucosides (Falcone Ferreyra et al., 2013), complete the maize maysin biosynthetic pathway.

Specialized metabolites, such as flavonoids, frequently provide a first level of defense against pathogens and herbivores (Field et al., 2006), and biological control often furnishes a more durable check against plant diseases than chemical pesticides (Bardin et al., 2015). The *Bacillus thuringiensis* (Bt) protein is only partially toxic to the CEW, and the development of resistance has been

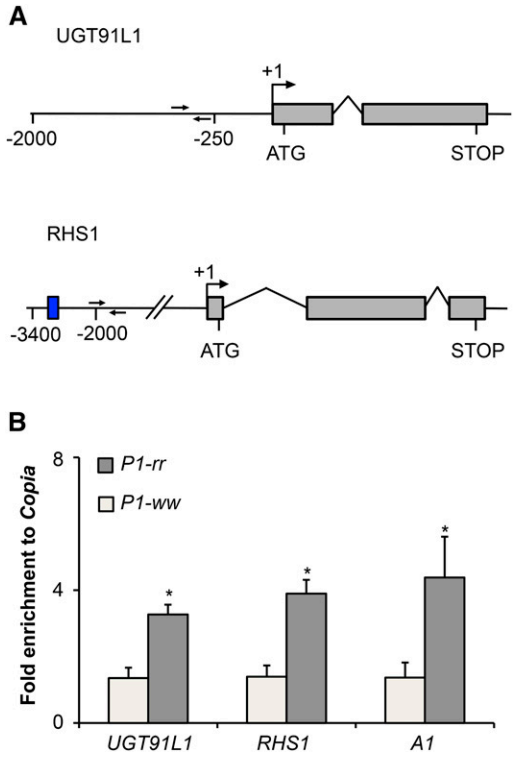

Figure 6. *UGT91L1* and *RHS1* Are Direct Targets of P1.

(A) *UGT91L1* and *RHS1* gene models. Exons are represented as gray boxes, introns as arched lines, and genomic regions as straight lines. Transcriptional start sites are depicted by perpendicular arrows at the +1 position; start (ATG) and stop (STOP) codon positions are also shown. MACS peaks estimated locations are indicated as a blue box. ChIP-qPCR primer locations are shown as head to head black arrows. Positions are given in base pairs from +1 transcriptional start sites.

(B) The bar plot corresponds to results from ChIP-qPCR experiments showing fold enrichment to *Copia* in *P1-rr* and *P1-ww* pericarps at 14 d after pollination for *UGT91L1* and *RHS1*, using *A1* as a positive control. Error bars correspond to SE of the mean, using six biological replicates ($n = 6$). Asterisks denote statistically significant differences between *P1-rr* and *P1-ww* at $P < 0.05$ (two-tailed *t* test).

reported (Reisig and Reay-Jones, 2015), suggesting a need to develop other methods of resistance. Moreover, recent analyses suggest a significant future threat of maize and other host crops by *Helicoverpa armigera* (Kriticos et al., 2015), which, similarly to *H. zea* (CEW) (Rector et al., 2002), is also sensitive to maysin. Thus, establishing the entire maysin biosynthetic pathway provides an opportunity to improve elite maize lines by marker-assisted breeding and also to transfer the pathway to other *Helicoverpa* susceptible plants. However, maysin and other *C*-glycosylflavones are also important in vegetative maize tissues for protection to UV-B exposure, characteristic of high-altitude maize landraces (Casati and Walbot, 2005). It is not yet known whether *Sm2* and *Sm1* participate in maysin accumulation in leaves in response to UV-B or whether other UGTs and rhamnose synthases are expressed in vegetative tissues. The maize B73 genome encodes ~160 UGTs, from which six are putative rhamnosyl transferases, based on phylogenetic analysis (Supplemental Figure 3). From these six rhamnosyl transferases, only UGT91L1 was included in the appropriate *Sm2* mapping interval and regulated by P1 (Supplemental Table 5).

The identity of *Sm2* as a rhamnosyl transferase was adequately predicted by the characterization of the pathway intermediates that accumulate in the *sm2* mutant (McMullen et al., 2004). The accumulation of derhamnosylmaysin, in addition to isoorientin, in the *sm2* mutant (Figure 2B) was proposed to reflect the ability of *Sm1* to also function on isoorientin (McMullen et al., 2004). However, this activity remains to be demonstrated.

While *Sm1* was also previously predicted to encode a glucose modification enzyme (McMullen et al., 2004), its identity as a rhamnose synthase (RHS1) came initially as a surprise. Rhamnose synthases are best known for the conversion of UDP-glucose to UDP-Rha, which is primarily used in the biosynthesis of cell wall components and for rhamnose-containing specialized metabolites (Kuhn et al., 2011; Lan et al., 2015). Our results demonstrate that rhamnose synthases can also function on glucose residues conjugated to a flavonoid instead of UDP, such as found in rhamnosylisoorientin (Figure 5). Similar to Arabidopsis RHM enzymes (Oka et al., 2007), RHS1 is predicted to encode a multidomain protein (Figure 5A) with an N-terminal-encoded dehydratase domain capable of converting the glucose residue in rhamnosylisoorientin to 4-keto-6-deoxy glucose, as found in maysin (Figure 5C). Interestingly, the conversion stops after the dehydration, suggesting perhaps that RHS1 lacks functional epimerase and keto-reductase activities characteristic of the C-terminal domain (Oka et al., 2007). However, we were able to show that RHS1 is capable of converting UDP-glucose to UDP-Rha by bioconversion assays in yeast (Supplemental Figure 7), indicating that there must be another reason why the reaction stops at maysin (Figure 5C). Whether this is a consequence of the additional rhamnose residue attached to position 2′ or whether this reflects that instead of a nucleotide-sugar the substrate is a flavonoid-sugar remains to be established. The fact that *sm1* mutants accumulate rhamnosylisorientin suggests that RHS1 is not the rhamnose synthase enzyme that provides UDP-Rha to UGT91L1 (Sm2) to generate rhamnosylisorientin. Thus, another rhamnose synthase encoded by the maize genome is responsible for the biosynthesis of UDP-Rha that is to be used by UGT91L1 or for cell wall biosynthesis (Supplemental Table 4). Nucleotide-sugar interconversions are part of central metabolism, yet RHS1 has clearly been co-opted for specialized metabolism, as our results indicate. This emergence of reshaped catalytic activities is at the core of the dramatic chemodiversity that plants display (Weng et al., 2012; Moghe and Last, 2015). It is currently unclear whether the ability to use flavonoid-glucose as a substrate is a general ability of plant multidomain rhamnose synthase enzymes or whether this is a unique activity of RHS1.

In conclusion, the results from these studies not only add novel enzymatic activities to one of the best-known plant specialized metabolism biosynthetic pathways, but also provide insight into how enzymes from primary metabolism are used to form important insecticidal specialized compounds. The challenge ahead is to use the knowledge acquired here in maize breeding programs aiming to increase resistance to emerging pests and to transfer the pathway to other plants that are victims of CEW.

METHODS

Maize Stocks and Plant Materials

sm1 and *sm2* stocks were obtained from the Maize Cooperation Stock Center. *sm1* stocks are as follows: 611A (*sm1-1*; *P1-rr*, *Pl1*, *sm1*); 611I (*sm1-2*; *P1-rr*, *tan1*, *py1*, *sm1*); 5809A (*sm1-3*; *sm1*, *rau*-6522*); M641G (sm1-4; *sm1-Brawn184*, *sm2-Brawn184*); M941F (*sm1-5*; *sm1*, *wx1*); and 607J, 607K, and 607L, which contained the alleles *sm1-Brawn168*, *sm1-Brawn178*, and *sm1-Brawn184*, respectively. *sm2* stocks are as follows: 201G (*sm2-1*; *sm2-Brawn180*); 201H (sm2-2; *sm2-Brawn189*); 201I (sm2-3; *sm2-Brawn190*); 201J (*sm2-4*; *sm2-Brawn191*), and 201K (*sm2-5*; *sm2-Brawn188*) (McMullen et al., 2004). *P1-rr* stock 65-CFS-305 and *P1-ww* stock 4Co43 were crossed into line A619 (*P1-ww*) as previously described (Morohashi et al., 2012). Briefly, the *P1-rr* CFS-305 allele in the 4Co43 background was introgressed into A619, which has no P1 or P2 expression, followed by six backcrosses and three selfing generations. The *P1-ww* allele in 4Co43 expressed the *P2* allele and was also introgressed into A619 (Morohashi et al., 2012). In all cases, silks were collected 2 to 3 d after emergence.

Chemicals

Isoorientin (luteolin-6-*C*-glucoside), rhamnosylisoorientin, and maysin were kindly provided by Michael McMullen (USDA-ARS) and Maurice Snook (Iowa State University). UDP-glucose, NAD^+, and NADPH were obtained from Sigma-Aldrich. The solvents methanol, acetonitrile, and water were obtained from Sigma-Aldrich.

Flavone Extraction

Fresh silks were freeze-dried overnight and ground in 100% (v/v) methanol (Sigma-Aldrich) to a final concentration of 50 mg dry tissue per mL and incubated overnight at −20°C. Silk extracts were filtered through a 0.2-μm membrane (Pall Nanosep MF) and stored at −20°C until further use (Casas et al., 2014).

HPLC Analysis

HPLC followed by photodiode array detection (HPLC-PDA) was performed on silks extracts as follows. Fresh silks were lyophilized overnight and ground in 100% (v/v) methanol (Sigma-Aldrich) to a final concentration of 50 mg of dry weight per mL and incubated overnight at −20°C. Silk extracts were filtered through a 0.2-μm membrane (Pall Nanosep MF), and 20 μL of the filtrate was injected into a Waters separation module W2690-5 and a W2996 PDA module following absorbance at 350 nm using a Symmetry C18 column (3.5 μm, 4.9 mm, 75 mm; Waters). The separation program started at an initial gradient of 80% solvent A–20% solvent B (solvent A: formic acid 0.1% [v/v] in water; solvent B: formic acid 0.1% [v/v] in acetonitrile) with a 0.75 mL/min flow to 100% solvent B in 15:33 min and kept for 1:20 min to finally return to initial conditions at 18:00 min (Casas et al., 2014).

Cloning of *UGT91L1*, *RHS1*, and *At-RHM1*

The $T7_{pro}$:His_6-UGT91L1 construct in pET28a was previously described (Falcone Ferreyra et al., 2013). The RHS1 (GRMZM2G031311) coding sequence was amplified from *P1-rr* silks using the OneStep RT-PCR kit (Qiagen). Briefly, 1 μg of RNA was incubated with 1× OneStep buffer, 1 mM of each dNTP, 0.5 μM of each primer, 0.5 μL RNase inhibitor, and 2 μL OneStep enzyme mix in a 50 μL final volume. The conditions for reverse transcription followed by PCR were as follow: 50°C for 30 min, 95°C for 15 min, 30 cycles of 94°C for 1 min, 53°C for 1 min, and 72°C for 2 min, followed by a final extension of 72°C for 10 min. The PCR product was purified, cloned into pENTR-D-TOPO vector (Invitrogen), sequenced, and used as template to clone full-length RHM1 into pET28a vector. PCR reactions were performed as described above for *UGT91L1* using primers listed in Supplemental Table 6; extension times were 150 s for the full-length gene. To clone *RHS1* and At-*RHM1* in the pGZ25 yeast expression vector, the respective coding regions were reamplified by PCR using the pENTR-D-TOPO clones previously generated as templates. In all cases, primers for coding sequences were designed based on the 5b.60b version of the maize genome (www.maizegdb.org).

The U15542 clone containing the At-*RHM1* coding sequence in pENTR-SD-D-TOPO was obtained from the ABRC.

UGT91L1 and *RHS1* were subcloned into protoplast expression vectors for transient expression fused to enhanced GFP, either at the N-terminal or C-terminal end, p1511BS and p1510BS, respectively, using a recombination cassette derived from the pK7FWG2 vector (Gateway compatible) and transferred into the pBluescript KS+ multicloning site. In all cases, vectors were sequenced to confirm that the fusions were in frame.

Yeast Strains and Transformation

Saccharomyces cerevisiae strain T334 (*ura3-52, leu2-3,112, △trp1::hisG, reg1-501, gal1, pep4-3, prb1-1122*) obtained from Claudia Spampinato at CEFOBI was used for expressing At-RHM1 and RHS1 (Lewis et al., 1998). Yeast strains were grown in YPD (1% [w/v] yeast extract, 2% [w/v] peptone, and 2% [w/v] glucose). Transformation was performed following the Trafo method (Gietz and Woods, 2002), and transformants were selected on synthetic complete media agar plates containing 2% (w/v) glucose without tryptophan (SCD-W). Transformed colonies appeared within 3 to 4 d of incubation at 30°C.

Rhamnosyl Transferase Activity Assay

To test for rhamnosyl transferase activity of UGT91L1, At-*RHM1* cloned into pGZ25 was transformed into yeast strain T334. Yeast cells were grown in SCD-W at 30°C for 48 h. Cells were harvested by centrifugation at 5000*g* for 5 min at room temperature, resuspended in 10 mM Tris-HCl (pH 7.5) with 1× of protease inhibitor (Thermo), and lysed with glass beads (425 to 600 μm; Sigma-Aldrich). Six series of 1-min periods of vortex-mixing alternating with 1 min incubation on ice were performed. The supernatants were collected after centrifugation and used as an enzymatic source. Total protein extracts from yeast expressing At-RHM1 or empty pGZ25 vector and total protein extracts from *Escherichia coli* expressing UGT91L1 or empty pET28a vector were prepared. To obtain *E. coli* crude extracts, *E. coli* Rosetta 2 (DE3) cells expressing UGT91L1 were grown as previously described (Falcone Ferreyra et al., 2013). Cells were harvested by centrifugation, resuspended in 50 mM KPi, pH 7.5, with 1 mM PMSF, sonicated, and centrifuged at 12,000*g* for 15 min at 4°C. Supernatants were used as an enzymatic source. In vitro RHM activity assays were performed in a reaction mix of 100 μL final volume containing 250 mM MOPS-NaOH, pH 7.5, 3 mM NAD^+, 3 mM NADPH, 3 mM UDP-glucose, and *S. cerevisiae* crude extract (absorbance at 600 nm of 5.0 to 7.5, harboring At-RHM1 or the pGZ25 empty vector; Oka et al., 2007). The reaction mixtures were incubated for 60 min at 30°C. The soluble fraction was extracted with chloroform and used as a UDP-Rha source for the following reaction of rhamnosyl transferase. Then, the following was added: 30 μL of *E. coli* protein extract (containing 85 μg of total protein, expressing UGT91L1 or empty pET28a), 0.15 mM isorientin in 50 mM KPi, pH 7.5, in a final volume of 200 μL. The reaction mixtures were incubated for 60 min at 30°C. Flavonoids were extracted with ethylacetate, vacuum dried, and resuspended in 100 μL 100% (v/v) methanol for LC-MS/MS analysis.

Maize Protoplast Preparation and Transformation

Second and third leaves from 14-d-old *sm1* and *sm2* etiolated seedlings were chopped to ~1-mm-thick pieces and digested in 3% (w/v) Cellulase RS, 0.6% (w/v) macerozyme R10 (Yakult Honsha Co.), 0.6 M mannitol,

10 mM KCl, 10 mM MES (pH 5.7), 5 mM $CaCl_2$, and 0.1% (w/v) BSA for 20 min under vacuum followed by 3 h gentle shaking at 30 g and 25°C in darkness. Protoplasts were released by shaking at 80*g* and 25°C in darkness and filtered through a 35-μm nylon mesh followed by centrifugation at 150*g* for 1 min at room temperature. Protoplasts were washed in ES buffer (0.6 M mannitol, 5 mM MES, pH 5.7, and 10 mM KCl) and counted using a hemocytometer under a microscope (Nikon SMZ1500, C-DSS115). Individual electroporations were performed on 10^5 protoplasts with 20 μg of total DNA per transformation for complementation assays, using 100 V/cm, 10 ms, and two pulses with a BTX Electro-Square-Porator T820. After electroporation, protoplasts were incubated for 18 to 22 h in the dark at room temperature before further analyses. Transformation efficiency was estimated as percentage of transformed cells following GFP expression using a fluorescence microscope (Nikon).

Complementation Assays of *salmon silks* Protoplasts and LC-MS/MS Analysis

Protoplasts from *sm1* and *sm2* lines were centrifuged for 2 min at low speed (~270*g*) at room temperature, the supernatant was removed, and protoplasts were resuspended in 100% (v/v) methanol (Sigma-Aldrich) and incubated for 10 min at 65°C (~10^6 initial cell number/mL corresponding to a pool of ten independent transformations). Following incubation, protoplasts were centrifuged for 5 min at 12,000*g* before filtering through a 0.2-μm membrane (Pall Nanosep MF) for further analysis by LC-MS/MS.

LC-MS/MS was performed in the Center for Applied Plant Sciences Targeted Metabolomics Laboratory on a linear ion trap quadrupole LC-MS/MS with a Q-Trap 5500 mass spectrometer (ABSciEX) in negative mode using multiple reaction monitoring following true standards. A Symmetry C18 column (3.5 μm, 4.9 mm, 75 mm; Waters) was used for a 15-μL injection volume with a flow of 1 mL/min (solvent A, water; solvent B, acetonitrile; Sigma-Aldrich). The program steps were 0.00 to 2.00 min 20% A; 2.00 to 9.00 min from 20 to 60% A; 9.10 to 11.00 min, 90% A; 11.00 to 11.10 min, 90 to 20% A; and 11.10 to 14.00 min, 20% A (Casas et al., 2014).

Gene Expression Analyses by RT- qPCR

Three independent biological replicates (i.e., obtained from three different individual plants) from *sm* mutants and *P1-rr* and *P1-ww* silk samples were snap-frozen in N_2 (l) and stored at −80°C. Total RNA was extracted using the RNeasy Plant Mini Kit followed by DNaseI treatment (Qiagen). cDNA was synthesized from 1 μg of total RNA using SuperScript Reverse Transcriptase II (Invitrogen) with oligo-$dT_{12\text{-}18}$ as primer. The resulting cDNA was used as template for PCR amplification in an iCycler iQ detection system with Optical System Software (v3.0a; Bio-Rad) using the intercalation dye SYBR Green I (Invitrogen) as a fluorescent reporter and Platinum Taq Polymerase (Invitrogen). Primers were designed to generate fragments of between 80 and 150 bp using Primer3 (Rozen and Skaletsky, 2000) (Supplemental Table 6). Transcript accumulated values were normalized to expression of *actin1* (GRMZM2G126010). Amplification conditions included 2 min initial denaturation at 94°C, 40 to 45 cycles of 94°C for 15 s, 57°C for 20 s, 72°C for 20 s, and a final extension step at 72°C for 5 min (Morohashi et al., 2012). Melting curves for each PCR product were determined by measuring the decrease of fluorescence with increasing temperature (from 65 to 95°C). To confirm the size of the PCR products and to check that they corresponded to a unique and expected PCR product, the final PCR products were separated on a 2% (w/v) agarose gel, stained with SYBR green (Invitrogen), and sequenced. Primers used for *UGT91L1* and *RHS1* are listed in Supplemental Table 6.

ChIP-qPCR

ChIP was performed by methods previously described (Morohashi and Grotewold, 2009; Morohashi et al., 2009; Falcone Ferreyra et al., 2010). Approximately 0.3 g of pericarps was fixed in Buffer A (0.4 M sucrose, 10 mM Tris-HCl, pH 8.0, 1 mM EDTA, 1 mM PMSF, and 0.1% [v/v] formaldehyde) for 10 min in vacuum. The cross-linking reaction was stopped by addition of 0.1 M glycine followed by an additional 5 min vacuum incubation. Fixed pericarps were washed and ground in liquid N_2. Nuclei were isolated using the plant nuclei isolation/extraction kit according to manufacturer's instructions (Sigma-Aldrich). Nuclear-enriched extracts were resuspended in 100 μL lysis buffer (50 mM HEPES, pH 7.5, 150 mM NaCl, 1 mM EDTA, 1% [v/v] Triton X-100, 0.1% [v/v] deoxycholate, 0.1% [w/v] SDS, 1 mM PMSF, and 10 mM sodium butyrate) and plant proteinase inhibitor cocktail (Sigma-Aldrich), followed by sonication with a Bioruptor (Diangenode) to ~300 bp of average fragment size.

For ChIP-qPCR analyses, and to correct for PCR bias, 1 pg of pUC19 plasmid was spiked into input and immunoprecipitated (ChIP) DNA. qPCR was performed using 0.1 to 1 μL of input or ChIPed DNA with Buffer J of the FailSafe PCR system (Epicentre Biotechnologies). ChIP-qPCR assays were performed using six biological replicates.

Phylogenetic Analysis of Maize Glycosyl Transferases

The phylogenetic tree was constructed using MEGA 6.0 software with the neighbor-joining method based on ClustalW multiple alignments (Larkin et al., 2007; Tamura et al., 2007). The bootstrap consensus tree was inferred from 1000 replicates and the branches corresponding to partitions corresponding to less than 50% bootstrap replicates are collapsed. Distances were computed using p-distance method and are in the units of the number of amino acid differences per site.

Sequencing of *sm1* and *sm2* Candidates

With the goal of identifying sequence variations that could potentially account for the salmon silk phenotype, each gene was divided in overlapping parts to cover the whole gene including the promoter region. The UGT91L1 genomic region covers 2.72 kb and was divided it into five overlapping regions (Supplemental Figure 4B). The RHS1 genomic region covers 3.94 kb, which was divided into nine overlapping regions (Supplemental Figure 6B).

We isolated genomic DNA from each line and performed PCR using the primer combinations described in Supplemental Table 7.

PCR Conditions

Briefly, 0.3 μg of genomic DNA from each *salmon silks* line was incubated with 1× buffer, 0.2 mM of each dNTP, 0.4 μM of each primer, and 1.5 units of Taq Polymerase in a 50 μL final volume. The amplification conditions were as follows: initial denaturation at 94°C for 3 min, followed by 30 cycles of 94°C for 1 min, 54°C for 45 s, 72°C for 90 s, and a final extension of 72°C for 5 min. The PCR products were purified and sent for sequencing at the Plant Microbe Genomics Facility at Ohio State University. Sequences were compared with version 2 of the maize genome (5b.60).

Statistical Analysis

All experiments performed in this study were at least done in biological triplicates. Data presented were analyzed using two-sided type 3 Student's *t* test, indicating statistically significant difference with letters at a P value of < 0.001, using Microsoft Excel.

Accession Numbers

Sequence data from this article can be found in in the Arabidopsis Genome Initiative under accession number At1g78570 (At-*RHM1*) and

in the maize genome sequence (version 3b.60 at http://ensembl.gramene.org/Zea_mays/Info/Index) under the following accession numbers: *UGT91L1* (GRMZM2G180283 corresponding to accession number ZEAMMB73_290687), *RHS1* (GRMZM2G031311 corresponding to accession number ZEAMMB73_283149), and *actin1* (GRMZM2G126010 corresponding to accession number ZEAMMB73_109222). Accession numbers used to generate phylogenetic tree in Supplemental Figure 3 are as follows: UGT708A6 (GRMZM2G162783); UGT708A5 (GRMZM2G162755); Bronze1 (GRMZM2G165390); UGT707A8 (GRMZM2G063550); GRMZM2G039129; AC199541.4_FG004; AC199541.4_FG007; AC199541.4_FG001; AC199541.4_FG002; GRMZM2G161335; GRMZM2G373124; GRMZM2G179063; GRMZM2G173315; GRMZM2G066067; GRMZM2G024131; GRMZM2G074395; GRMZM2G031138; GRMZM2G328224; GRMZM2G098892; GRMZM2G098890; GRMZM2G363545; GRMZM2G160523; GRMZM2G416045; GRMZM2G168474; GRMZM2G120016; GRMZM2G021786; GRMZM2G035755; GRMZM2G082249; GRMZM2G009125; GRMZM5G870067; GRMZM2G086925; GRMZM2G154558; GRMZM2G083935; GRMZM2G334336; GRMZM2G463996; GRMZM2G173926; GRMZM2G047910; GRMZM2G110816; GRMZM2G006565; GRMZM2G306328; GRMZM2G171548; GRMZM2G022212; GRMZM2G170228; GRMZM5G834303; GRMZM2G113794; GRMZM2G415973; GRMZM2G022242; GRMZM2G022266; GRMZM2G343426; GRMZM2G075387; GRMZM2G163519; GRMZM2G056335; GRMZM2G372068; GRMZM2G156127; GRMZM2G324466; GRMZM2G131928; GRMZM2G363554; GRMZM2G178209; GRMZM2G479038; GRMZM2G338465; GRMZM2G055446; GRMZM2G105991; GRMZM2G083130; GRMZM2G135722; GRMZM2G061289; GRMZM2G061321; GRMZM2G073376; GRMZM2G004858; GRMZM2G381025; GRMZM2G122072; GRMZM2G051683; GRMZM2G073244; GRMZM5G888620; GRMZM2G319965; GRMZM2G106443; GRMZM2G085054; GRMZM2G085854; GRMZM2G426415; GRMZM2G007012; GRMZM2G389944; GRMZM2G128504; GRMZM2G046994; GRMZM2G041699; GRMZM2G169628; GRMZM2G470524; GRMZM5G832805; GRMZM5G896260; GRMZM2G301148; GRMZM2G130256; GRMZM2G156026; GRMZM2G007795; GRMZM2G304712; GRMZM2G030821; GRMZM2G337048; GRMZM2G417945; GRMZM2G449019; GRMZM2G148277; GRMZM2G325014; GRMZM2G325023; GRMZM2G008935; GRMZM2G151332; GRMZM2G049798; GRMZM2G476049; GRMZM2G132706; GRMZM2G091176; GRMZM2G159918; GRMZM2G432291; GRMZM2G118657; GRMZM2G067361; GRMZM2G050748; GRMZM2G383404; GRMZM2G458776; GRMZM2G316030; GRMZM2G051474; GRMZM2G145670; GRMZM2G440902; GRMZM2G037545; GRMZM2G082037; AC206788.3_FG015; GRMZM2G058314; GRMZM2G159404; GRMZM5G815665; GRMZM5G892627; GRMZM2G097030; GRMZM2G117878; GRMZM2G175910; GRMZM2G078465; GRMZM2G089241; GRMZM2G395508; GRMZM2G095261; GRMZM2G155911; GRMZM2G455075; GRMZM2G096412; GRMZM2G060993; GRMZM2G174192; GRMZM2G457929; GRMZM2G095280; GRMZM2G022101; GRMZM2G042865; GRMZM2G095807; GRMZM2G010987; GRMZM2G110511; GRMZM2G130119; GRMZM2G036409; GRMZM2G111344; GRMZM2G403740; GRMZM2G008539; GRMZM2G099740; GRMZM2G344993; GRMZM2G475884; AC234524.1_FG005; GRMZM2G043295; GRMZM2G113653; GRMZM2G035282; GRMZM2G063042; GRMZM5G854655; GRMZM2G426242; and GRMZM2G067424.

Supplemental Data

Supplemental Figure 1. Biochemical characterization of *sm2* mutants.

Supplemental Figure 2. Biochemical characterization of *sm1* mutants.

Supplemental Figure 3. Phylogenetic analysis of putative UGT proteins from maize.

Supplemental Figure 4. Molecular characterization of *UGT91L1* in *sm2* lines.

Supplemental Figure 5. Constructs for mutant protoplast complementation.

Supplemental Figure 6. Molecular characterization of *RHS1* in *sm1* lines.

Supplemental Figure 7. *RHS1* encodes UDP-rhamnose synthase.

Supplemental Table 1. Characteristics of available *salmon silks* alleles.

Supplemental Table 2. P1-activated genes in the *sm2* interval.

Supplemental Table 3. P1-activated genes in the *sm1* interval.

Supplemental Table 4. Putative rhamnose synthases present in the maize genome.

Supplemental Table 5. Putative rhamnosyl transferases clustering together with UGT91L1.

Supplemental Table 6. Primers used in this study.

Supplemental Table 7. Primers used for sequencing candidate genes.

Supplemental Data Set 1. Alignment used to generate the phylogeny presented in Supplemental Figure 3.

ACKNOWLEDGMENTS

This project was supported by the Agriculture and Food Research Initiative competitive grant 2015-67013-22810 of the USDA National Institute of Food and Agriculture and FONCyT Grant PICT 2013-0082 to M.L.F.-F. and by a grant from the National Science Foundation (IOS-1125620) to E.G. We thank Mike McMullen and the Maize Genetics Cooperation Stock Center for providing the seed stocks used in this study and the ABRC for the At RHM1 construct. We thank the Center for Applied Plant Sciences (CAPS) Targeted Metabolomics Laboratory, especially Jean-Christophe Cocuron, for his contributions in the LC-MS/MS method development and Ana P. Alonso for her expertise in sugar and sugar-nucleotide analysis support and discussions. We thank Claudia Spampinato (CEFOBI-CONICET) for providing the T344 yeast strain. We also thank Rob Last, Venkat Gopalan, Keith Slotkin, and David Mackey for their valuable feedback to this study. Lastly, we thank Mike McMullen for numerous discussions and ideas over the years, the three anonymous reviewers of this study for their insightful comments, and the CAPS Computational Biology Laboratory for RNA-seq analysis discussions. M.L.F.-F., E.R., and P.C. are members of the Researcher Career of the Consejo Nacional de Investigaciones Científicas y Técnicas (CONICET).

AUTHOR CONTRIBUTIONS

M.I.C., M.L.F.-F., P.C., and E.G. designed research. M.I.C., M.L.F.-F., N.J., E.R., J.E., and T.W. performed research. M.I.C., M.L.F.-F., and M.K.M.-G analyzed data. M.I.C. and E.G. wrote the article. All authors read and approved the final manuscript.

Received January 8, 2016; revised May 2, 2016; accepted May 23, 2016; published May 24, 2016.

REFERENCES

Anderson, E.G. (1921). The Inheritance of Salmon Color in Maize. Master's thesis (Ithaca, NY: Cornell University).

Anderson, E.G., and Emerson, R.A. (1923). Pericarp studies in maize I. The inheritance of pericarp colors. Genetics **8:** 466–476.

Bailey, D.M., and Bailey, R.M. (1938). The relation of the pericarp to tenderness in sweet corn. P. Am. Soc. Hortic. Sci. **36:** 555–559.

Bardin, M., Ajouz, S., Comby, M., Lopez-Ferber, M., Graillot, B., Siegwart, M., and Nicot, P.C. (2015). Is the efficacy of biological control against plant diseases likely to be more durable than that of chemical pesticides? Front. Plant Sci. **6:** 566.

Brazier-Hicks, M., Evans, K.M., Gershater, M.C., Puschmann, H., Steel, P.G., and Edwards, R. (2009). The C-glycosylation of flavonoids in cereals. J. Biol. Chem. **284:** 17926–17934.

Byrne, P.F., McMullen, M.D., Snook, M.E., Musket, T.A., Theuri, J.M., Widstrom, N.W., Wiseman, B.R., and Coe, E.H. (1996). Quantitative trait loci and metabolic pathways: genetic control of the concentration of maysin, a corn earworm resistance factor, in maize silks. Proc. Natl. Acad. Sci. USA **93:** 8820–8825.

Casas, M.I., Duarte, S., Doseff, A.I., and Grotewold, E. (2014). Flavone-rich maize: an opportunity to improve the nutritional value of an important commodity crop. Front. Plant Sci. **5:** 440.

Casati, P., and Walbot, V. (2005). Differential accumulation of maysin and rhamnosylisoorientin in leaves of high altitude landraces of maize after UV-exposure. Plant Cell Environ. **28:** 788–799.

Cocciolone, S.M., Chopra, S., Flint-Garcia, S.A., McMullen, M.D., and Peterson, T. (2001). Tissue-specific patterns of a maize Myb transcription factor are epigenetically regulated. Plant J. **27:** 467–478.

Coe, E.H., Jr. (2001). The origins of maize genetics. Nat. Rev. Genet. **2:** 898–905.

Elliger, C.A., Chan, B.C., and Waiss, A.C., Jr. (1980). Flavonoids as larval growth inhibitors. Naturwissenshaften **67:** 358–360.

Emerson, R.A. (1917). Genetical studies of variegated pericarp in maize. Genetics **2:** 1–35.

Falcone Ferreyra, M.L., Rius, S., Emiliani, J., Pourcel, L., Feller, A., Morohashi, K., Casati, P., and Grotewold, E. (2010). Cloning and characterization of a UV-B-inducible maize flavonol synthase. Plant J. **62:** 77–91.

Falcone Ferreyra, M.L., Rodriguez, E., Casas, M.I., Labadie, G., Grotewold, E., and Casati, P. (2013). Identification of a bifunctional maize C- and O-glucosyltransferase. J. Biol. Chem. **288:** 31678–31688.

Falcone Ferreyra, M.L., Emiliani, J., Rodriguez, E.J., Campos-Bermudez, V.A., Grotewold, E., and Casati, P. (2015). The identification of maize and Arabidopsis type I FLAVONE SYNTHASEs links flavones with hormones and biotic interactions. Plant Physiol. **169:** 1090–1107.

Field, B., Jordán, F., and Osbourn, A. (2006). First encounters–deployment of defence-related natural products by plants. New Phytol. **172:** 193–207.

Gietz, R.D., and Woods, R.A. (2002). Transformation of yeast by lithium acetate/single-stranded carrier DNA/polyethylene glycol method. Methods Enzymol. **350:** 87–96.

Giraud, M.F., and Naismith, J.H. (2000). The rhamnose pathway. Curr. Opin. Struct. Biol. **10:** 687–696.

Grotewold, E., Athma, P., and Peterson, T. (1991). Alternatively spliced products of the maize P gene encode proteins with homology to the DNA-binding domain of myb-like transcription factors. Proc. Natl. Acad. Sci. USA **88:** 4587–4591.

Grotewold, E., Chamberlin, M., Snook, M., Siame, B., Butler, L., Swenson, J., Maddock, S., St Clair, G., and Bowen, B. (1998). Engineering secondary metabolism in maize cells by ectopic expression of transcription factors. Plant Cell **10:** 721–740.

Kriticos, D.J., Ota, N., Hutchinson, W.D., Beddow, J., Walsh, T., Tay, W.T., Borchert, D.M., Paula-Moreas, S.P., Czepak, C., and Zalucki, M.P. (2015). The potential distribution of invading *Helicoverpa armigera* in North America: Is it just a matter of time? PLoS One **10:** 1–24.

Kuhn, B.M., Geisler, M., Bigler, L., and Ringli, C. (2011). Flavonols accumulate asymmetrically and affect auxin transport in Arabidopsis. Plant Physiol. **156:** 585–595.

Lan, W., Lu, F., Regner, M., Zhu, Y., Rencoret, J., Ralph, S.A., Zakai, U.I., Morreel, K., Boerjan, W., and Ralph, J. (2015). Tricin, a flavonoid monomer in monocot lignification. Plant Physiol. **167:** 1284–1295.

Larkin, M.A., et al. (2007). ClustalIW and ClustalIX version 2. Bioinformatics **23:** 2947–2948.

Levings, C.S. (1972). A new anthocyanidin in maize: luteolinidin. Maize Cooperation Newsletters **46:** 149–151.

Lewis, L.K., Kirchner, J.M., and Resnick, M.A. (1998). Requirement for end-joining and checkpoint functions, but not RAD52-mediated recombination, after EcoRI endonuclease cleavage of *Saccharomyces cerevisiae* DNA. Mol. Cell. Biol. **18:** 1891–1902.

Liu, H., Du, Y., Chu, H., Shih, C.H., Wong, Y.W., Wang, M., Chu, I.K., Tao, Y., and Lo, C. (2010). Molecular dissection of the pathogen-inducible 3-deoxyanthocyanidin biosynthesis pathway in sorghum. Plant Cell Physiol. **51:** 1173–1185.

McMullen, M.D., Kross, H., Snook, M.E., Cortés-Cruz, M., Houchins, K.E., Musket, T.A., and Coe, E.H., Jr. (2004). Salmon silk genes contribute to the elucidation of the flavone pathway in maize (*Zea mays* L.). J. Hered. **95:** 225–233.

Moghe, G.D., and Last, R.L. (2015). Something old, something new. Conserved enzymes and the evolution of novelty in plant specialized metabolism. Plant Physiol. **169:** 1512–1523.

Morohashi, K., et al. (2012). A genome-wide regulatory framework identifies maize pericarp color1 controlled genes. Plant Cell **24:** 2745–2764.

Morohashi, K., and Grotewold, E. (2009). A systems approach reveals regulatory circuitry for Arabidopsis trichome initiation by the GL3 and GL1 selectors. PLoS Genet. **5:** e1000396.

Morohashi, K., Xie, Z., and Grotewold, E. (2009). Gene-specific and genome-wide ChIP approaches to study plant transcriptional networks. Methods Mol. Biol. **553:** 3–12.

Morris, C.E., and Sands, D.C. (2006). The breeder's dilemma–yield or nutrition? Nat. Biotechnol. **24:** 1078–1080.

Oka, T., Nemoto, T., and Jigami, Y. (2007). Functional analysis of *Arabidopsis thaliana* RHM2/MUM4, a multidomain protein involved in UDP-D-glucose to UDP-L-rhamnose conversion. J. Biol. Chem. **282:** 5389–5403.

Rector, B.G., Snook, M.E., and Widstrom, N.W. (2002). Effect of husk characters on resistance to corn earworm (Lepidoptera: Noctuidae) in high-maysin maize populations. J. Econ. Entomol. **95:** 1303–1307.

Reisig, D.D., and Reay-Jones, F.P. (2015). Inhibition of *Helicoverpa zea* (Lepidoptera: Noctuidae) growth by transgenic corn expressing Bt toxins and development of resistance to Cry1Ab. Environ. Entomol. **44:** 1275–1285.

Reiter, W.D., and Vanzin, G.F. (2001). Molecular genetics of nucleotide sugar interconversion pathways in plants. Plant Mol. Biol. **47:** 95–113.

Rice, P., Longden, I., and Bleasby, A. (2000). EMBOSS: the European Molecular Biology Open Software Suite. Trends Genet. **16:** 276–277.

Rozen, S., and Skaletsky, H. (2000). Primer3 on the WWW for general users and for biologist programmers. Methods Mol. Biol. **132:** 365–386.

Sidorenko, L.V., Li, X., Cocciolone, S.M., Chopra, S., Tagliani, L., Bowen, B., Daniels, M., and Peterson, T. (2000). Complex structure of a maize Myb gene promoter: functional analysis in transgenic plants. Plant J. **22:** 471–482.

Tamura, K., Dudley, J., Nei, M., and Kumar, S. (2007). MEGA4: Molecular Evolutionary Genetics Analysis (MEGA) software version 4.0. Mol. Biol. Evol. **24:** 1596–1599.

Waiss, A.C., Jr., Chan, B.G., Elliger, C.A., Wiseman, B.R., McMillian, W.W., Widstrom, N.W., Zuber, M.S., and Keaster, A.J. (1979). Maysin, a flavone glycoside from corn silks with antibiotic activity toward corn earworm. J. Econ. Entomol. **72:** 256–258.

Watt, G., Leoff, C., Harper, A.D., and Bar-Peled, M. (2004). A bifunctional 3,5-epimerase/4-keto reductase for nucleotide-rhamnose synthesis in Arabidopsis. Plant Physiol. **134:** 1337–1346.

Wei, F., et al. (2009). The physical and genetic framework of the maize B73 genome. PLoS Genet. **5:** e1000715.

Weng, J.K., Philippe, R.N., and Noel, J.P. (2012). The rise of chemodiversity in plants. Science **336:** 1667–1670.

Widstrom, N.W., and Snook, M.E. (1998a). Genetic variation for maysin and its analogs in crosses among corn inbreds. Crop Sci. **38:** 372–375.

Widstrom, N.W., and Snook, M.E. (1998b). A gene controlling biosynthesis of isoorientin, a compound in corn silks antibiotic to the corn earworm. Entomol. Exp. Appl. **89:** 119–124.

Wiseman, B.R., Snook, M.E., Isenhour, D.J., Mihm, J.A., and Widstrom, N.W. (1992). Relationship between growth of corn earworm and fall armyworm larvae (Lepidoptera: Noctuidae) and maysin concentration in corn silks. J. Econ. Entomol. **85:** 2473–2477.

Yin, Y., Huang, J., Gu, X., Bar-Peled, M., and Xu, Y. (2011). Evolution of plant nucleotide-sugar interconversion enzymes. PLoS One **6:** e27995.

The Plant Cell, Vol. 28: 1984–1987, August 2016, www.plantcell.org

CORRECTION[OPEN]

Casas, M.I., Falcone-Ferreyra, M.L., Jiang, N., Mejía-Guerra, M.K., Rodríguez, E., Wilson, T., Engelmeier, J., Casati, P., and Grotewold, E. (2016). Identification and characterization of maize *salmon silks* genes involved in insecticidal maysin biosynthesis. Plant Cell **28:** 1297–1309.

We inadvertently added an extra -CH_2- to the structures of UDP-4-keto-6-deoxy glucose and UDP-rhamnose within the structure of maysin and these other molecules, a mistake that was kindly brought to our attention by Ying Zeng (Kunming Institute of Botany, Chinese Academy of Sciences, Yunnan, China). This slightly affected Figures 1, 2A, and 5 but did not have any effect on any of the results or conclusions of the study.

For ease of comparison, the original and corrected versions of the three figures affected by this mistake are presented below with the positions of the errors and corrections marked with red arrows.

www.plantcell.org/cgi/doi/10.1105/tpc.16.00602

Figure 1. (original)

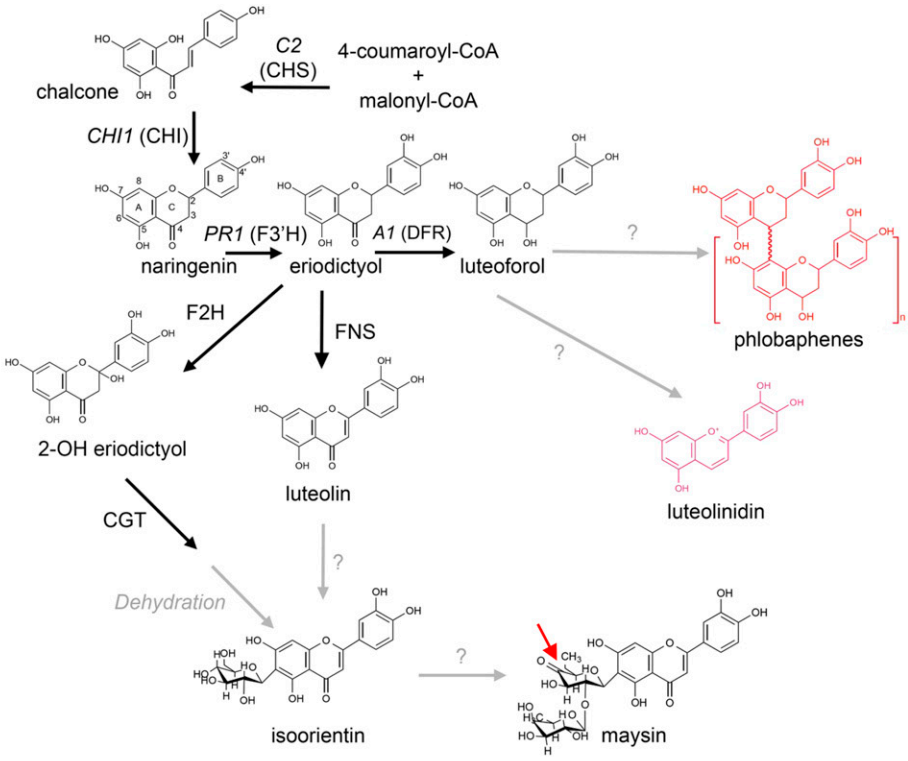

Figure 1. (corrected)

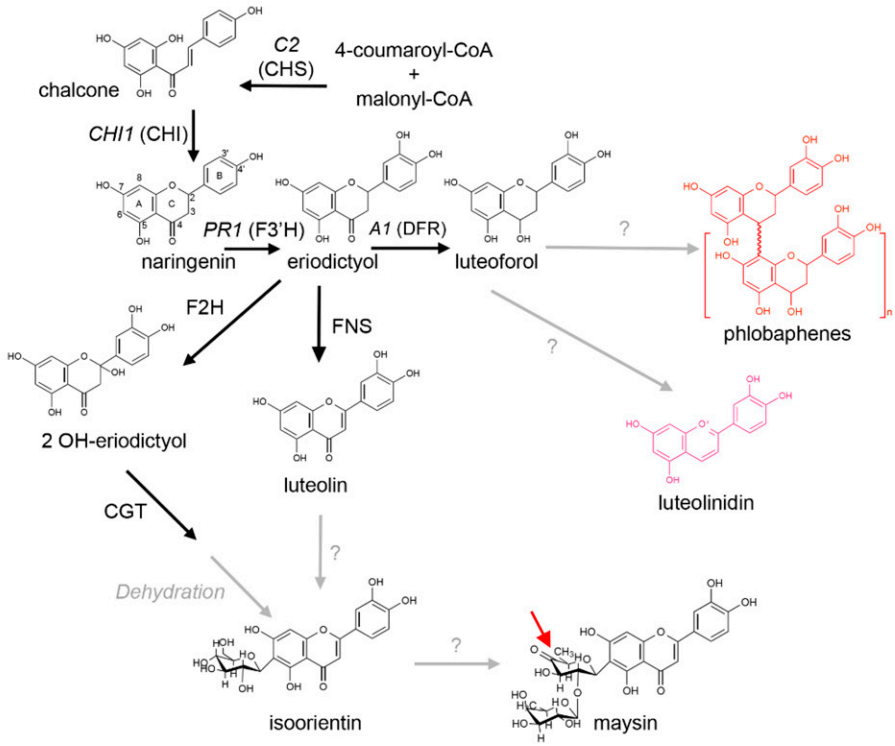

Figure 1. Proposed 3-Deoxyflavonoid Biosynthetic Pathway.

Condensation of *p*-coumaroyl-CoA and malonyl-CoA by chalcone synthase (CHS; *C2*) results in naringenin chalcone, which is then converted to naringenin by chalcone isomerase (CHI; encoded by *CHI1*). Naringenin is converted to eriodictyol by a flavanone-3′-hydroxylase (F3′H1; encoded by *PR1*), which could then be converted to the flavone luteolin by a flavone synthase (FNS; *FNSI-1*) (Falcone Ferreyra et al., 2015). Eriodictyol is converted

Figure 2A (original).

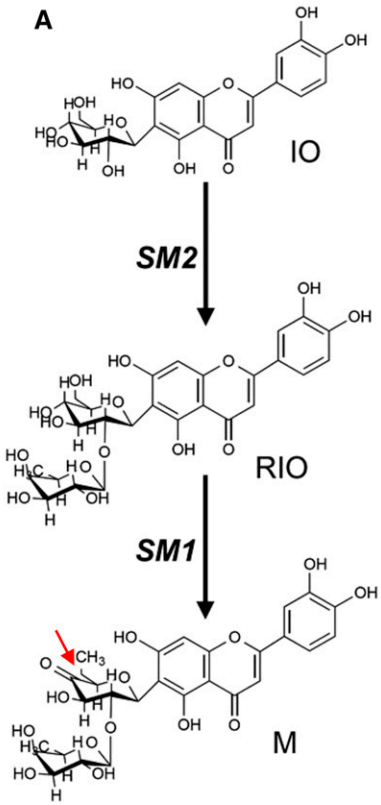

Figure 2A (corrected).

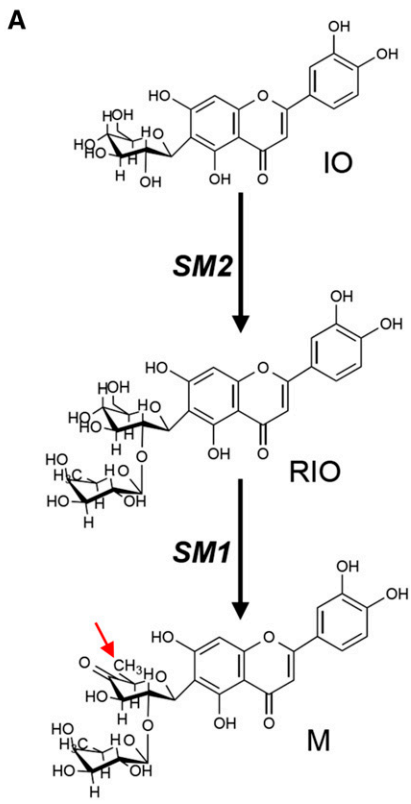

Figure 2. Biochemical Analysis of *sm* Lines.

(A) Proposed pathway for maysin formation. The reaction from IO to RIO is proposed to be mediated by *sm2* and the dehydration of RIO to maysin (M) by *sm1*.

Figure 1. (continued).

to isoorientin (*C*-glycosyl flavone) by a flavanone-2-hydroxylase (F2H; *CYP93G5*) (Morohashi et al., 2012) and a *C*-glucosyl transferase (CGT; *UGT708A6*) (Falcone Ferreyra et al., 2013). The proposed steps for conversion of isoorientin to maysin involve at least two enzymatic conversions by as yet uncharacterized enzymes. Eriodictyol is also converted to luteoforol (flavan-4-ol) by a dihydroflavonol reductase (DFR; *A1*) and subsequently to luteolinidin (3-deoxy anthocyanidin) by what is thought to be an ANS-like enzyme (Liu et al., 2010) or is polymerized into phlobaphenes. Enzymes identified are shown in black, and proposed steps are in gray. Phlobaphenes are shown in red, and 3-deoxyanthocyanidins are shown in pink.

Figure 5 (original).

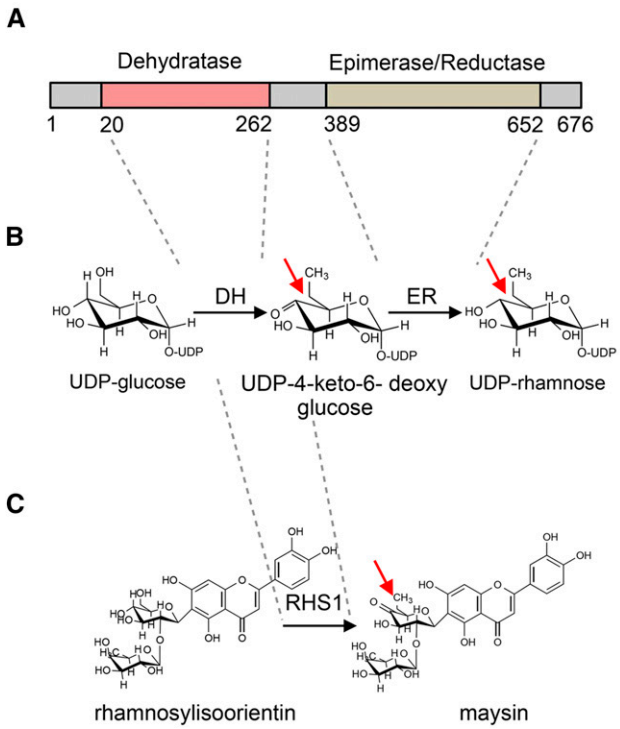

Figure 5 (corrected).

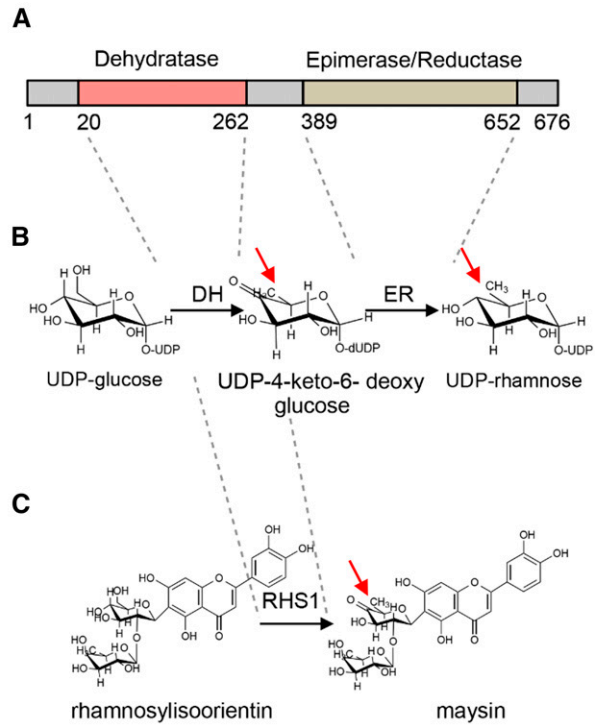

Figure 5. Proposed Mechanism for RHS1 as *sm1* Candidate.

RHS1 contains two domains characteristic of plant rhamnose synthases.
(A) The N-terminal domain between residues 20 and 262 corresponds to a NAD^+-dependent dehydratase and the C-terminal domain corresponds to an epimerase/reductase between residues 389 and 652.
(B) UDP-rhamnose biosynthesis starts with a dehydration step to form the UDP-4-keto-6-deoxy glucose intermediate, which is then converted to UDP-rhamnose by an epimerization reduction step.
(C) Proposed mechanism for RHS1 involvement in maysin biosynthesis by dehydrating the glucose moiety in rhamnosylisoorientin.

Editor's note: the corrected figures and accompanying text were reviewed by members of *The Plant Cell* editorial board.

Identification and Characterization of Maize *salmon silks* Genes Involved in Insecticidal Maysin Biosynthesis

María Isabel Casas, María Lorena Falcone-Ferreyra, Nan Jiang, María Katherine Mejía-Guerra, Eduardo Rodríguez, Tyler Wilson, Jacob Engelmeier, Paula Casati and Erich Grotewold

Plant Cell 2016;28;1297-1309; originally published online May 24, 2016;
DOI 10.1105/tpc.16.00003